

We are IntechOpen, the world's leading publisher of Open Access books Built by scientists, for scientists

4,500

Open access books available

118,000

International authors and editors

130M

Downloads

Our authors are among the

154

Countries delivered to

TOP 1%

most cited scientists

12.2%

Contributors from top 500 universities



WEB OF SCIENCE™

Selection of our books indexed in the Book Citation Index
in Web of Science™ Core Collection (BKCI)

Interested in publishing with us?
Contact book.department@intechopen.com

Numbers displayed above are based on latest data collected.
For more information visit www.intechopen.com



Bio-Inspired Microstrip Antenna

Alexandre Jean René Serres,
Georgina Karla de Freitas Serres,
Paulo Fernandes da Silva Júnior,
Raimundo Carlos Silvério Freire,
Josiel do Nascimento Cruz,
Tulio Chaves de Albuquerque,
Maciel Alves Oliveira and
Paulo Henrique da Fonseca Silva

Additional information is available at the end of the chapter

<http://dx.doi.org/10.5772/intechopen.69766>

Abstract

In the last few years, bio-inspired solutions have attracted the attention of the scientific community. Several world-renowned institutions have sponsored and created laboratories in order to understand the forms, functions and behavior of living organisms. Some methods can be highlighted in the search for geometric representation of the shapes found in the nature, the fractal geometry, the polar geometry, and the superformula of Gielis. This chapter is focusing on bio-inspired microstrip antennas, especially on leaf-shaped antennas from the Gielis superformula that open a vast research field for more compact antennas with low visual impact.

Keywords: bio-inspired, Gielis superformula, compact antenna, leaf-shaped antennas, visual impact

1. Introduction

From the 1990s, with the advent of the Internet, the popularization of portable terminals (laptops, mobile phones, etc.) favored the telecommunications industry and the infrastructure of networks experienced a remarkable growth [1, 2]. When the information age emerges from an increasingly networked world, the digital information, and communication technology

permeate the society and are increasingly important to their development [3, 4]. Modern wireless applications demand esthetic, multifunctional, and portable terminals that operating in multiple frequency bands and can integrate different wireless services: 4G, Wi-Fi, Bluetooth, NFC, GPS and so on. Future trends toward 5G systems also require enhanced mobile broadband for emergent applications [5].

With the rapid advance of wireless communication systems, the use of antennas in base stations and portable terminals must meet increasingly stringent criteria, such as miniaturization, integration with other systems, and multiband or broadband operation [1–4]. Due its attractive features, low-profile microstrip antennas (MSA) and arrays are well suitable to meet the demands of fixed or mobile wireless applications [6–9].

Antenna parameter specifications change according to application. Indeed, fixed antennas must have high gain, stable radiation pattern, and bandwidth tolerance; embedded antennas should be efficient in radiation and possess larger beam width [3]. In short-range UWB wireless systems, the antenna bandwidth exceeds the lesser of 500 MHz or 20% of the center frequency [9]. Thus, impedance bandwidth, gain, radiation pattern, and polarization are fundamental parameters for antenna designers to take into account.

A trend in the application of antennas for modern wireless systems is the use of compact antennas with stable radiation coverage over a wideband [2–4]. An antenna must be compact in many situations: embedded antennas, wearable antennas, camouflaged antennas, and so on. However, most often an antenna electrically small narrows the impedance bandwidth, reduces gain, and limits control of the resulting radiation pattern [4, 6, 9].

Various institutions around the world have invested resources and established research centers with focus on biologically inspired engineering as the Massachusetts Institute Technology, the London College, and the Harvard University, for example. This research branch looks in nature similar solution to the problems encountered in engineering. With appropriate adjustments, it is possible to adapt the solutions used by the nature of the engineering problems [10]. According to [11], the development of a bioinspired methodology requires three steps: identification of analogies, with structures and methods that are similar; understanding, detailed modeling of actual biological behavior; and engineering, which is the process of model simplification and adjustments to technical applications.

The researches that use the bio-inspired geometry for the development of antennas are recent and can be divided into two groups: antennas with bio-inspired geometries in animals and antennas with bio-inspired geometries in plants. Bio-inspired antennas in animals try to use internal organs or external parts of the animals which work analogously to the operation of the antennas used in the communication systems. A biomimetic antenna in the shape of a bat's ear [12] can be cited, a biologically inspired electrically small antenna arrays that mimic the hearing mechanism of such insects [13], an antenna system based on the wasp's curved antennas [14] and a biologically inspired vascular antenna reconfiguration mechanism [15]. Research on antennas with bio-inspired plant geometries uses the plants or part of them (stem, leaves, and flowers) to develop antennas for various frequencies and technologies. The study of microstrip antennas with models bio-inspired on leaves (leaf-shaped antennas) has aroused

the interest of researchers due to the good results. The leaves present similar characteristics to fractals as, for example, the reduction of the total dimensions with the increase of perimeter. Furthermore, the leaves have a light-harvesting reaction center complex, i.e., an array of antennas capable of operating in the visible light range (400–700 nm) with characteristics which analog to satellite dishes. The main purpose of the leaf shape is to capture the sunlight to transform it in chemical energy by a photosynthesis process. The bioinspired on leaves open a vast research field for more compact antennas with low visual impact. Among the published works, the following can be highlighted. A leaf-shaped monopole antenna with an extremely wide bandwidth is introduced in Ref. [16] and a leaf-shaped bowtie slot antenna for UWB applications in Ref. [17]. A band-notched tulip antenna for UWB applications is presented in Ref. [18] and a wide-band tulip-loop antenna in Ref. [19]. More recently, a MIMO antenna using castor leaf-shaped quasi-self-complementary elements for broadband applications and a bio-inspired design of directional leaf-shaped printed monopole antennas for 4G 700 MHz band are presented in Refs. [20] and [21], respectively.

This chapter discusses the design of innovative bio-inspired microstrip antennas with fractal, polar, and Gielis shapes, which are optimized for wireless applications. Section 2 presents the different methods to generate bio-inspired shapes. In section 3 are presented some applications including esthetic wearable antennas and antenna arrays. In this last section, the results obtained from the Gielis superformula are highlighted due to the simplicity and flexibility of the formulation. Simulations are performed using ANSYS Electronics Desktop. Measurements of prototypes are compared to simulations and classical designs as circular printed monopole antenna in some cases.

2. Bio-inspired shapes

2.1. Fractal and polar transformations

From a mathematical point of view, a fractal refers to a set in Euclidean space with specific properties, such as self-similarity or self-affinity, simple and recursive definition, fractal dimension, irregular shape, and natural appearance [22]. Fractal geometry is the study of sets with these properties, which are too irregular to be described by calculus or traditional Euclidian geometry language [22, 23].

Fractals are resort to conventional classes, such as geometrical fractals, algebraic fractals, and stochastic fractals [24]. Two common methods used to generate mathematical fractals are iterated function systems (IFS) and Lindenmayer systems [22–25].

Lindenmayer system (or L-system) was initially conceived to model growth phenomena in biological organisms [26]. An L-system grammar performs an initial string of symbols (axiom) and includes a set of production rules that may be applied to the symbols (letters of the L-system alphabet) to generate new strings.

In **Figure 1** are shown four examples of fractal iterations using IFS and L-system.

Like fractals, polar transformations give rise to a wide class of shapes. A polar transformation is defined in this chapter through a vector function $\vec{v}(t) = (x(t), y(t))$, $t \geq 0$, that is, for each real value, t is associated with a vector in \mathfrak{R}^2 , Eq. (1). An example of an esthetic polar transformation is defined by Eq. (2) and presented in **Figure 2** for k varying up to $k = 24$ petals.

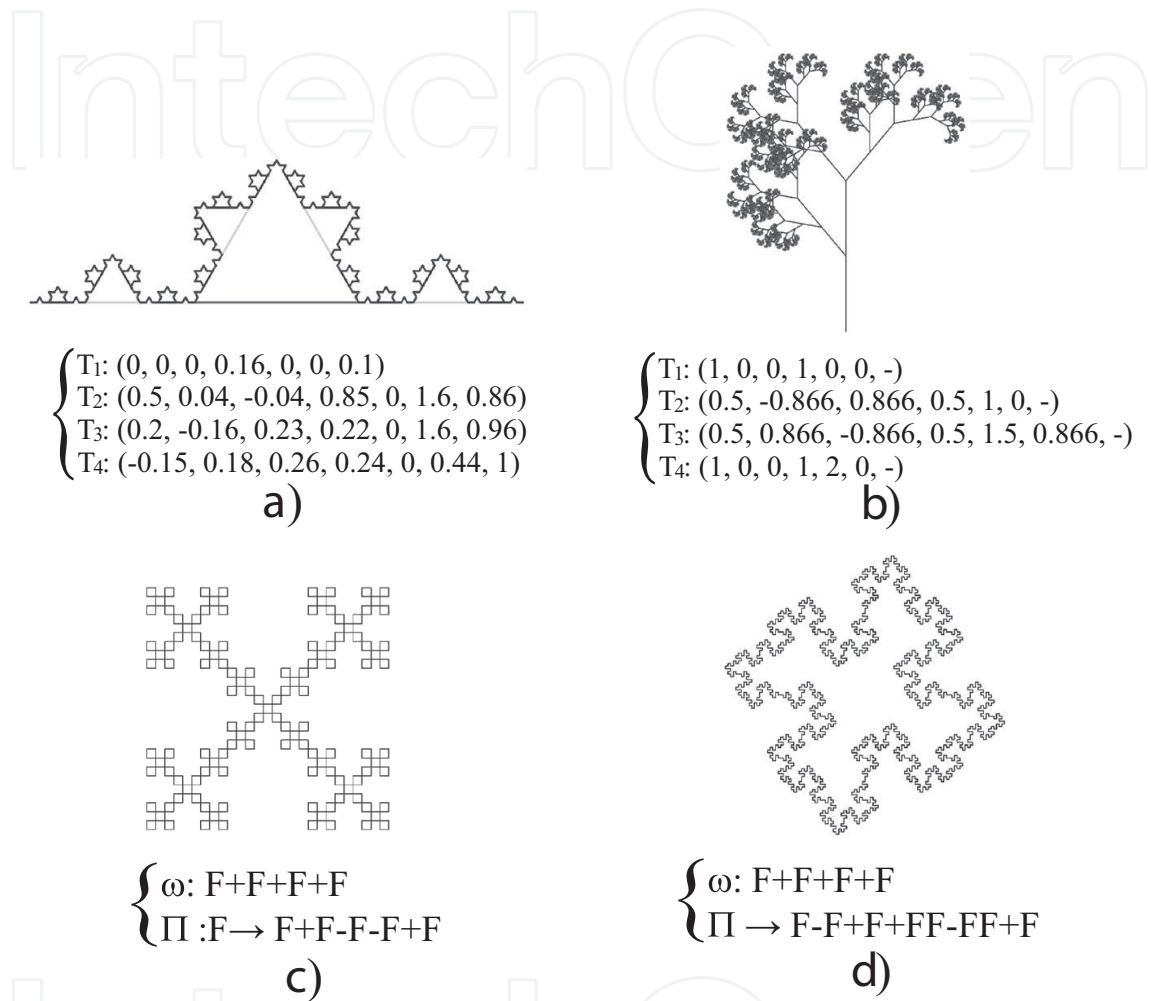


Figure 1. IFS and L-system prefractals: (a) Koch curve; (b) modified Barnsley fern; (c) Koch island; (d) Minkowski island.

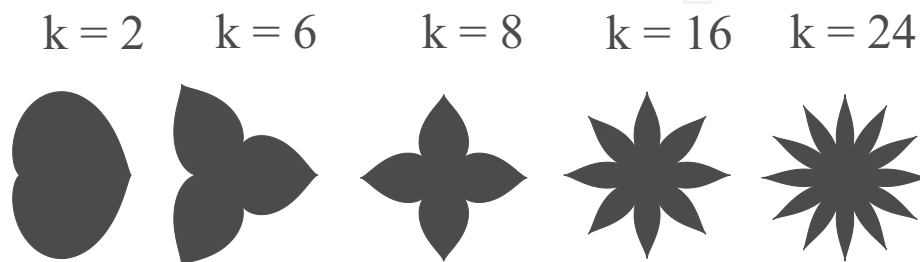


Figure 2. Esthetic space-filling polar transformation for k varying up to $k = 24$.

$$\begin{aligned} \vec{v}(t): I &\rightarrow \mathfrak{R}^n \\ t &\rightarrow \vec{v}(t) \end{aligned} \tag{1}$$

$$\vec{v}(t) = \left(1 + \frac{\cos(t)}{2}\right) \cdot \left(\cos\left(\frac{2t - \sin(2t)}{k}\right), \sin\left(\frac{2t - \sin(2t)}{k}\right)\right), \quad 0 \leq t \leq k\pi \tag{2}$$

2.2. Gielis superformula

The superformula is a generalization of the superellipse and was first proposed by Johan Gielis in 2003 [27]. With this model, it is possible to describe mathematically a wide variety of natural and abstract forms, such as leaf and flower shapes, for example. Gielis started from the concept of superellipses (3) and obtained the superformula (4), which is based on the idea that many natural forms can be interpreted as modified circles. To obtain this result, it was used polar coordinates, replacing $x = r \cdot \cos(\varphi)$ and $y = r \cdot \sin\varphi$ in addition to introducing the argument $m/4$, which confers rotational symmetry in some structures, and the possibility of using different values of exponent n for each term (through n_1, n_2, n_3).

$$\left|\frac{x}{a}\right|^n + \left|\frac{y}{b}\right|^n = 1 \tag{3}$$

$$r(\varphi) = \frac{1}{\left\{ \left[\left(\left| \frac{1}{a} \cos\left(\varphi \frac{m}{4}\right) \right| \right)^{n_2} + \left(\left| \frac{1}{b} \sin\left(\varphi \frac{m}{4}\right) \right| \right)^{n_3} \right]^{\frac{1}{n_1}} \right\}} \tag{4}$$

From the manipulation of the six parameters (a, b, m, n_1, n_2, n_3) of (4), called the Gielis superformula, it is possible to generate and modify several shapes. The superformula can also be multiplied by other mathematical functions, generating other forms. In order to illustrate the possibilities of the superformula, some examples of star shaped, leaf shaped, butterfly shaped, and flower shaped were generated. These shapes can be seen, with all the parameters used, in **Tables 1–4**, respectively.




| Shape | Superformula parameters | | | | | | Function | ϕ |
|---|-------------------------|-----|-----|-------|-------|-------|----------|----------|
| | a | b | m | n_1 | n_2 | n_3 | | |
|  | 1 | 1 | 7 | 10 | 6 | 6 | 1 | $0:2\pi$ |
|  | 10 | 10 | 5 | 2 | 7 | 7 | 1 | $0:2\pi$ |
|  | 1 | 1 | 5 | 2 | 13 | 13 | 1 | $0:2\pi$ |

Table 1. Star-shaped geometries.




| Superformula parameters | | | | | | | | |
|---|-----|-----|-----|-------|-------|-------|----------|----------|
| Shape | a | b | m | n_1 | n_2 | n_3 | Function | ϕ |
|  | 1 | 1 | 2 | 500 | 1000 | 1000 | 1 | $0:2\pi$ |
|  | 2 | 2 | 3 | 1 | 1 | 1 | 1 | $0:2\pi$ |
|  | 2 | 2 | 2 | 1 | 1 | 2 | 1 | $0:2\pi$ |

Table 2. Leaf-shaped geometries.




| Superformula parameters | | | | | | | | |
|---|-----|-----|-----|-------|-------|-------|---------------------|----------|
| Shape | a | b | m | n_1 | n_2 | n_3 | Function | ϕ |
|  | 1 | 1 | 4 | 0.2 | 0.5 | 15 | $ \cos(m\varphi) $ | $0:2\pi$ |
|  | 1 | 1 | 4 | 0.2 | 0.5 | 15 | 1 | $0:2\pi$ |
|  | 1 | 1 | 4 | 0.2 | 0.5 | 15 | $ \cos(2m\varphi) $ | $0:2\pi$ |

Table 3. Butterfly-shaped geometries.




| Superformula parameters | | | | | | | | |
|---|-----|-----|-----|-------|-------|-------|--------------------|----------|
| Shape | a | b | m | n_1 | n_2 | n_3 | Function | ϕ |
|  | 1 | 1 | 10 | 0.1 | 10 | 0.01 | 1 | $0:2\pi$ |
|  | 10 | 1 | 100 | 1 | 0 | 4 | 1 | $0:2\pi$ |
|  | 1 | 1 | 2.5 | 100 | 2.7 | 2.7 | $ \cos(m\varphi) $ | $0:2\pi$ |

Table 4. Flower-shaped geometries.

3. Applications in microstrip antennas

The bio-inspired shapes are generated using the software MATLAB® in format DXF.

The simulations were performed with the commercial software ANSYS Electronics Desktop™, and the measurements in the Radiometry Laboratory of the Federal University of Campina Grande, with the VNA Agilent Technologies, model E5071C-280 (9 kHz–8.5 GHz) and the Measurements Laboratory of the Federal Institute of Paraíba (IFPB), Campus João Pessoa, using

the VNA of Agilent Technologies model N5230A (300 kHz–13.5 GHz). The characterization of denim substrate was performed by the probe method using a VNA of Agilent model E5071C (300 kHz–20 GHz).

The rigid antennas were designed using a low-cost fiberglass laminate (FR4) as dielectric substrate with a thickness of $h = 1.5$ mm, dielectric constant of $\epsilon_r = 4.4$, and loss tangent of 0.02.

The wearable bio-inspired antennas were designed using a denim as dielectric substrate with a thickness of $h = 1$ mm, dielectric constant of $\epsilon_r = 2.14$ and loss tangent of 0.08, and flexible copper.

3.1. Wearable bio-inspired prefractal antennas

The use of wearable antennas are necessary some characteristics as easy interaction with the body, low visual impact, preferably low cost, and flexible structure [28], and for this reason, the materials used in the manufacture of the wearable antennas must follow some requirements: easy interaction with the body, flexible structure, reduced visual impact, and preferably low cost [28].

Figure 3 shows the development of wearable textile patch antenna generated by L-systems with $k = 4$ interactions. **Figure 3(a)** illustrates the original bio-inspired shape, and **Figure 3(b)**

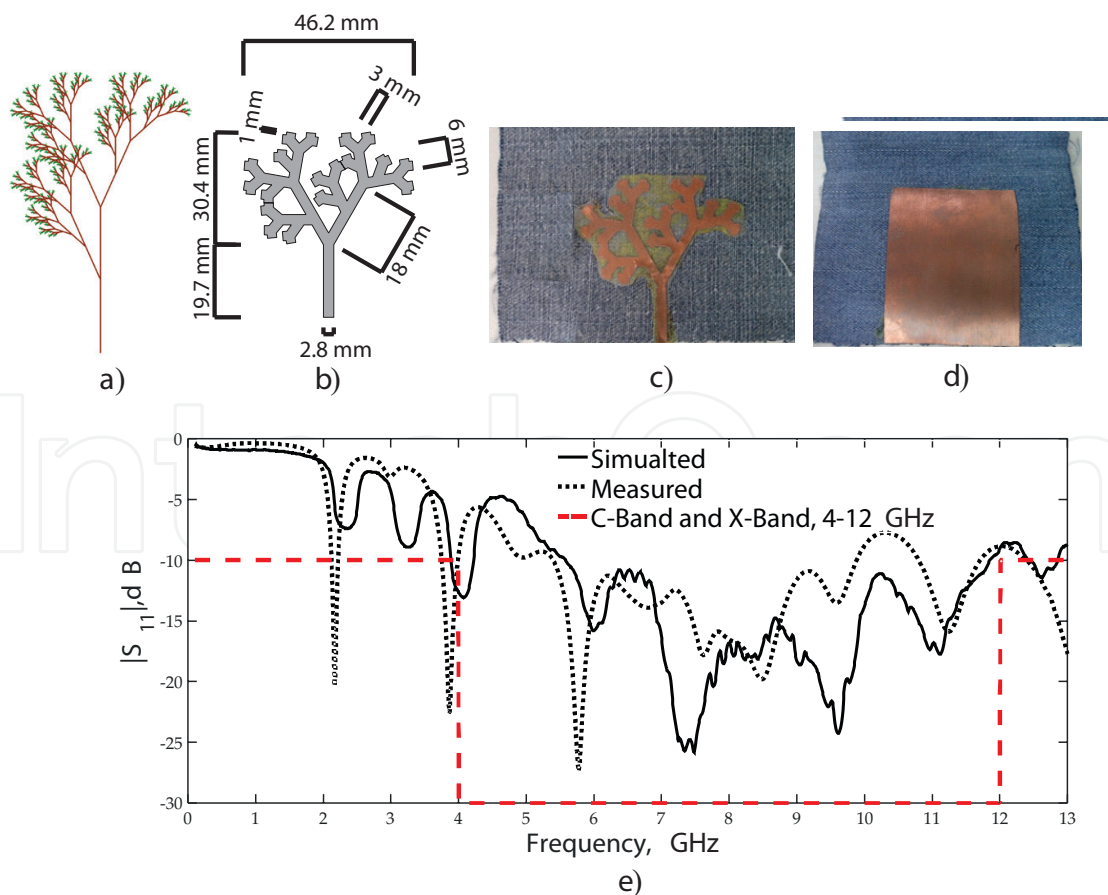


Figure 3. Development of wearable textile patch antenna generated by L-systems: (a) original shape, (b) image generated by MATLAB, (c) top layer prototype, (d) bottom layer prototype and (e) comparison between simulated and measured return loss.

presents the image generated by MATLAB® using turtle algorithm. **Figure 3(c)** and **(d)** show the top and bottom layers of the prototype built, respectively.

As observed in **Figure 3(e)**, the antenna presents an UWB behavior operating between the C-Band (4–8 GHz) and X-Band (8–12 GHz), with measured bandwidth of 5.95 GHz (5.9–1.85 GHz), and good relationship between simulated and measured results, with difference in bandwidth of 17%.

3.2. Bio-inspired polar microstrip antennas

Figure 4 shows frequency resonance of bio-inspired polar microstrip antenna for k -interactions ($k = 1, 8, 12, 16, 24, 32, 40, 48, 56, 64$) and the comparison of measured $|S_{11}|$ parameter, with prototype images. The proposed of bio-inspired patch antennas is based on a circle patch antenna with displaced microstrip line feed, and quarter-wave transformer, with dimensions calculated accordingly [7, 9].

Figure 4 shows the $|S_{11}|$ parameters measured of the polar antennas to $k = 8, 16$, and 24 . We noted that the increase of the patch perimeter by use of polar interaction provides a reduction of the resonant frequencies, similar to the fractal compartment.

Figure 5 shows the use of polar transformer in development of the array patch antenna with 4 petals, $k = 8$ interactions. The polar array presented good response, with simulated and measured results closed, and loss return less than -45 dB, bandwidth of 101 MHz, cover the WLAN band in 2.4 GHz.

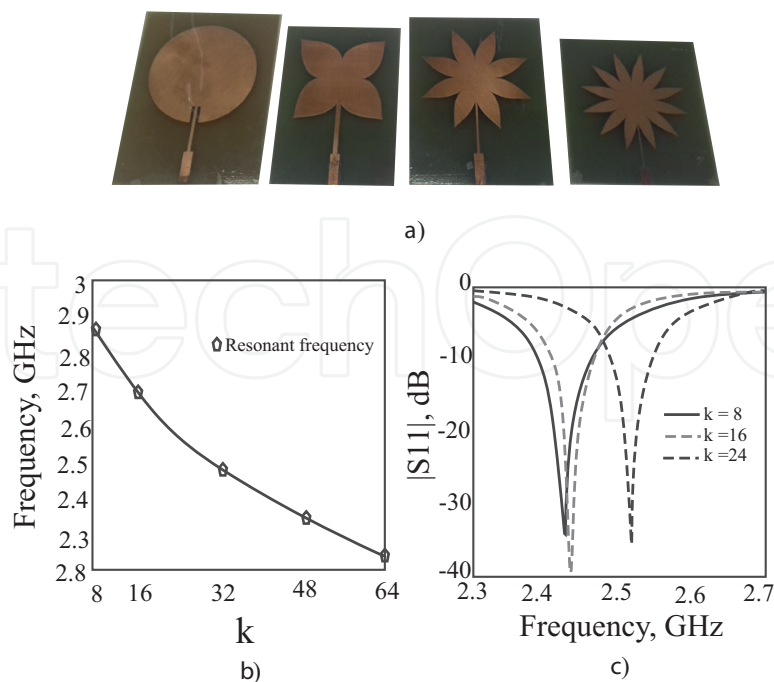


Figure 4. Interactions of bio-inspired polar microstrip patch antenna: (a) prototypes; (b) resonant frequency vs interactions and (c) return loss for $k = 8, 16$ and 24 .

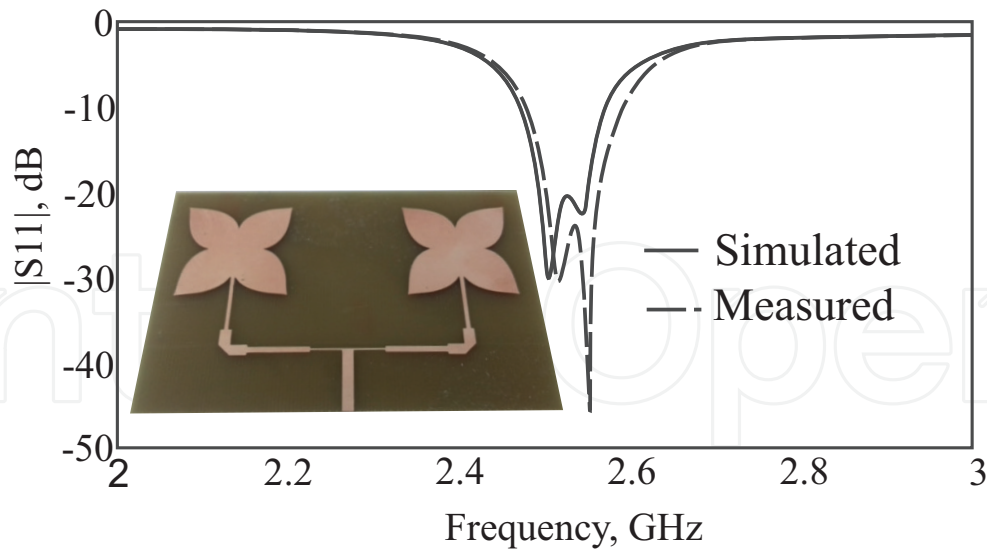


Figure 5. Polar microstrip patch antenna 1×2 array.

3.3. Leaf-shaped antennas from Gielis superformula

3.3.1. Tulip flower-shaped antenna

The image of the tulip flower with three petals was generated by the Gielis superformula using the software MATLAB®, with values: $m = 2$, $n_1 = 400$, n_2 and $n_3 = 1200$, a and $b = 1$. In Figure 6 are shown the dimensions of the petals, the design simulated, and the prototype antenna.

The radiation element is composed of one central petal and two lateral petals with an inclination of 25°. The antenna was designed for a first resonance frequency at 2.1 GHz, with wavelength of $\lambda \approx 13$ mm, which was used as approximated dimension between the edge and the center of the structure.

Figure 7 presents the comparison of simulated and measured $|S_{11}|$ parameter of the tulip flower-shaped antenna. In Table 5, it can be observed the measured and simulated values of

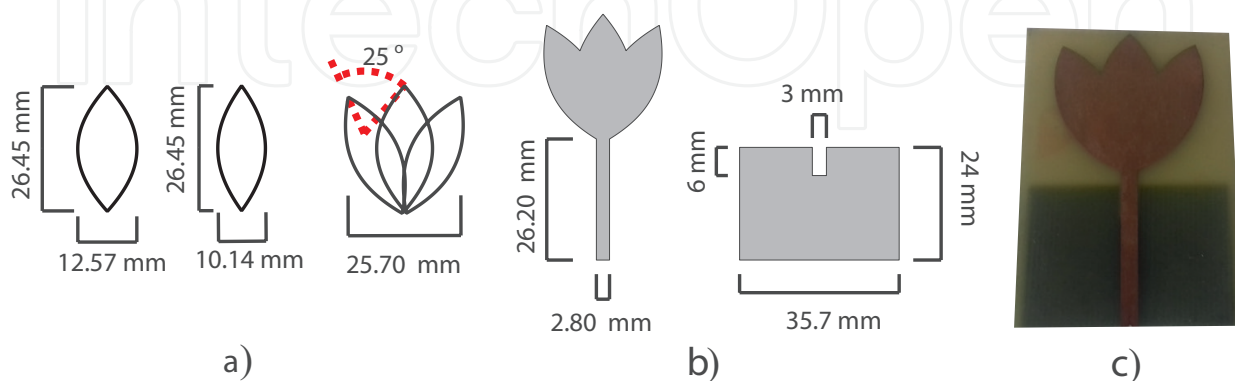


Figure 6. Tulip flower-shaped antenna for UWB applications: (a) petals exported in DXF format; (b) simulated structure top and bottom and (c) prototype.

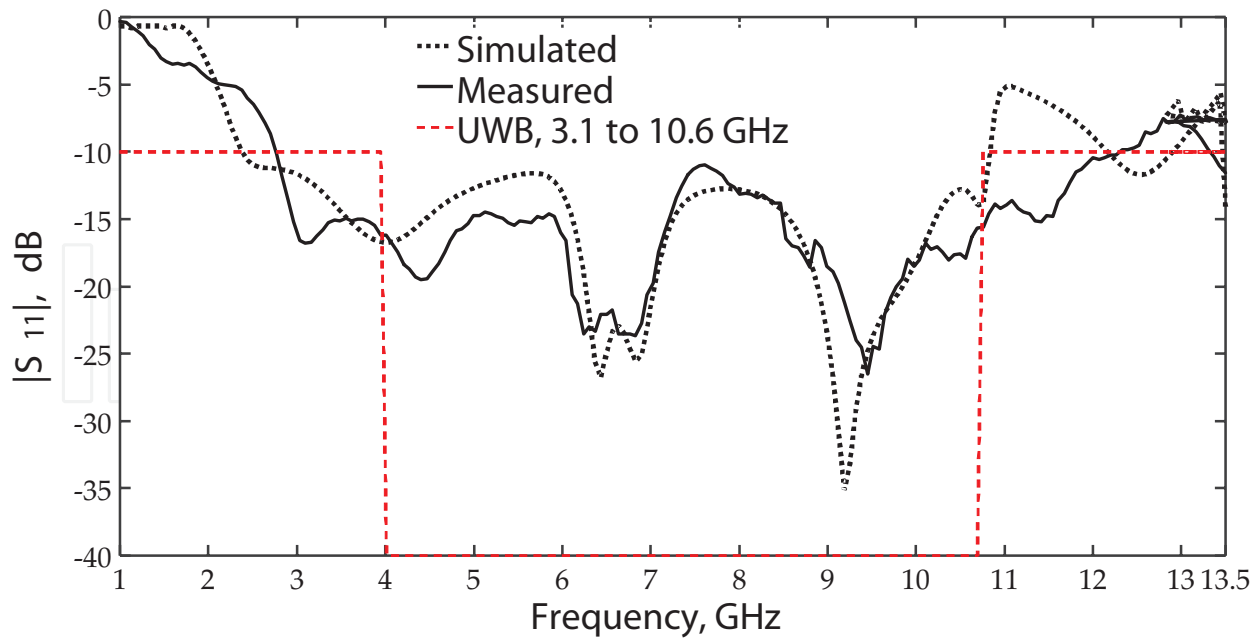


Figure 7. Comparison between simulated and measured return loss of the tulip flower-shaped antenna.

| | <i>Antenna</i> | BW (GHz) | f_1 (GHz) | f_2 (GHz) |
|---|----------------|-----------------|-------------|-------------|
| 1 | Simulated | 9.45 | 1.37 | 10.82 |
| 2 | Measured | 9.56 | 2.77 | 12.33 |

Table 5. Measured and simulated values of resonant frequencies and bandwidth of the bio-inspired antenna.

resonant frequencies and bandwidth of the bio-inspired antenna. It can be noted that both antennas comply with the FCC parameters with a bandwidth greater than 7.5 GHz (3.1–10.6 GHz).

The 3D radiation patterns simulated for the frequencies of 6.3 and 8.6 GHz can be observed in **Figure 8(a)** and **(b)**. The 2D radiation patterns simulated for the same frequencies can be observed in **Figure 8(c)** and **(d)** with radiation pattern measured in semi-anechoic chamber for $\Phi = 90^\circ$. The results cover the FCC parameters, with omnidirectional radiation pattern, half power beam width (HPBW) greater than 60° , maximum gain in broadside direction, and current density of 6 A/m^2 .

3.3.2. Jasmine flower-shaped antenna

Based on a circular planar monopole antenna (PMA) with a radius of 10.71 mm, a bio-inspired printed monopole antenna with the geometry of jasmine flower with 10 petals was designed. The image of the jasmine flower with 10 petals with 1 mm long was generated by Gielis superformula using the software MATLAB®, with values: $m = 10$, $n_1 = -2$, n_2 and $n_3 = 1.2$, a and $b = 1$, and the parameters: $m = 10$, $n_1 = 8$, n_2 and $n_3 = -0.6$, a and $b = 1$ for petals with 7 mm long.

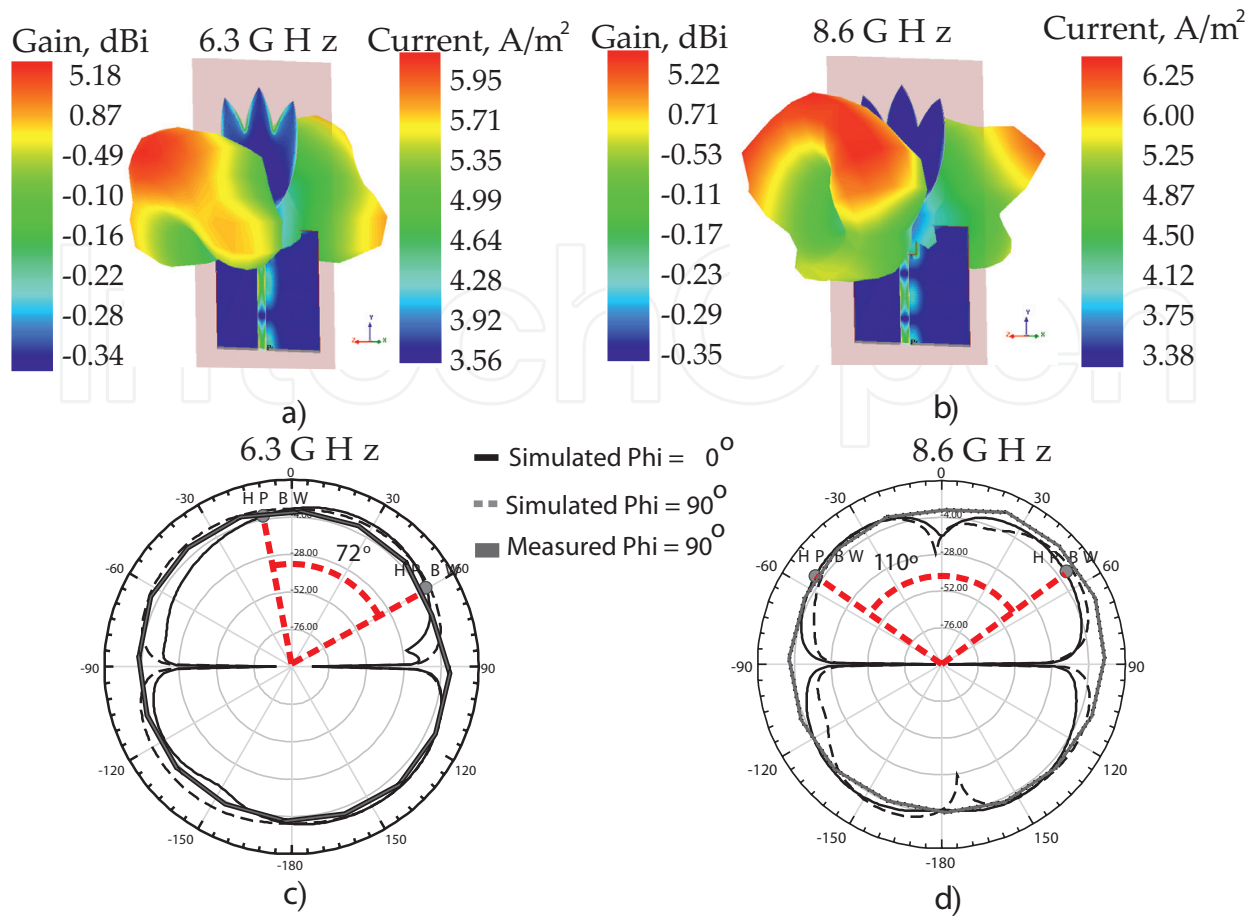


Figure 8. Radiation pattern: (a) far-field 3D with gain in dBi and current density in A/m^2 at 6.3 GHz; (b) far-field 3D with gain in dBi and current density in A/m^2 at 8.6 GHz; (c) 2D, E-plane ($\phi = 0^\circ$) and H-plane ($\phi = 90^\circ$) with HPBW indication at 6.3 GHz; (d) 2D, E-plane ($\phi = 0^\circ$) and H-plane ($\phi = 90^\circ$) with HPBW indication at 8.6 GHz.

In **Figure 9** are shown the shapes generated, simulated structures with dimensions, and prototypes of the proposed antennas. The use of the bio-inspired geometry provided a reduction of 11.3% in comparison with the classical PMA.

As seen in **Figure 10**, for the circular PMA, measured and simulated results are close, indicating convergence between the designed and built prototypes.

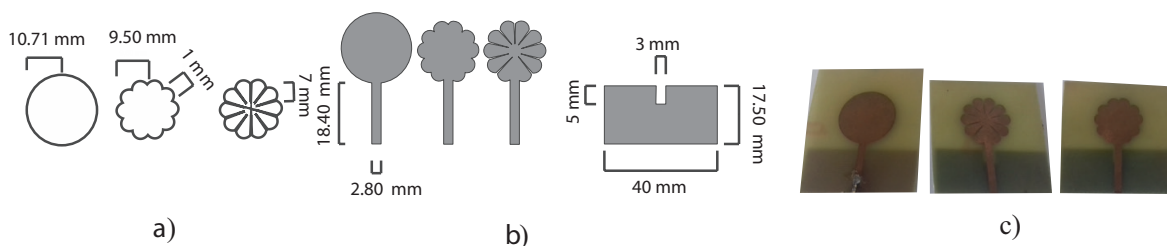


Figure 9. Jasmine flower-shaped antenna: (a) shapes exported in DXF format; (b) simulated structures, top and bottom; (c) prototypes.

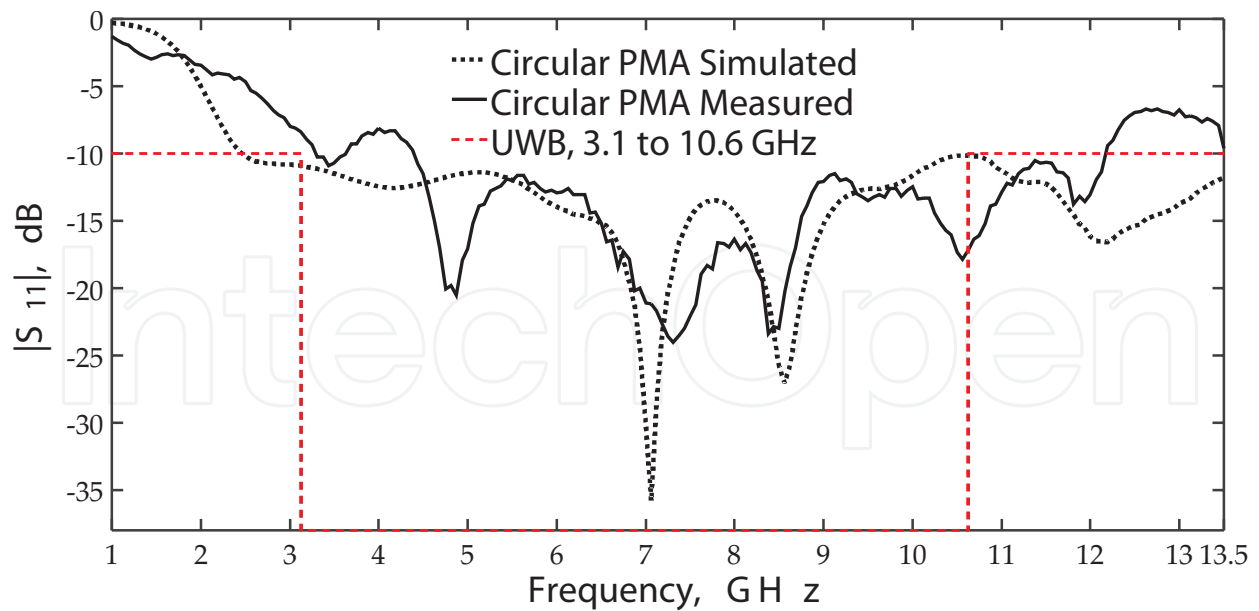


Figure 10. Comparison between simulated and measured results for designed circular printed monopole antenna.

In order to validate the simulations, two prototypes of bio-inspired PMA were built with petal lengths of 1 and 7 mm. The comparisons between simulated and measured results are shown in Figures 11 and 12.

It can be seen, from the Figures 11 and 12, that increasing the length defining the petals allows a reduction in the radius of the patch element in 11.30% and promotes the modification of the resonance frequency. The antenna with 7 mm presented an operating range within the range of the X-Band frequency. The measurements of the return loss of the circular PMA and the bio-inspired antenna with a petal length of 7 mm present a higher bandwidth than the simulation.

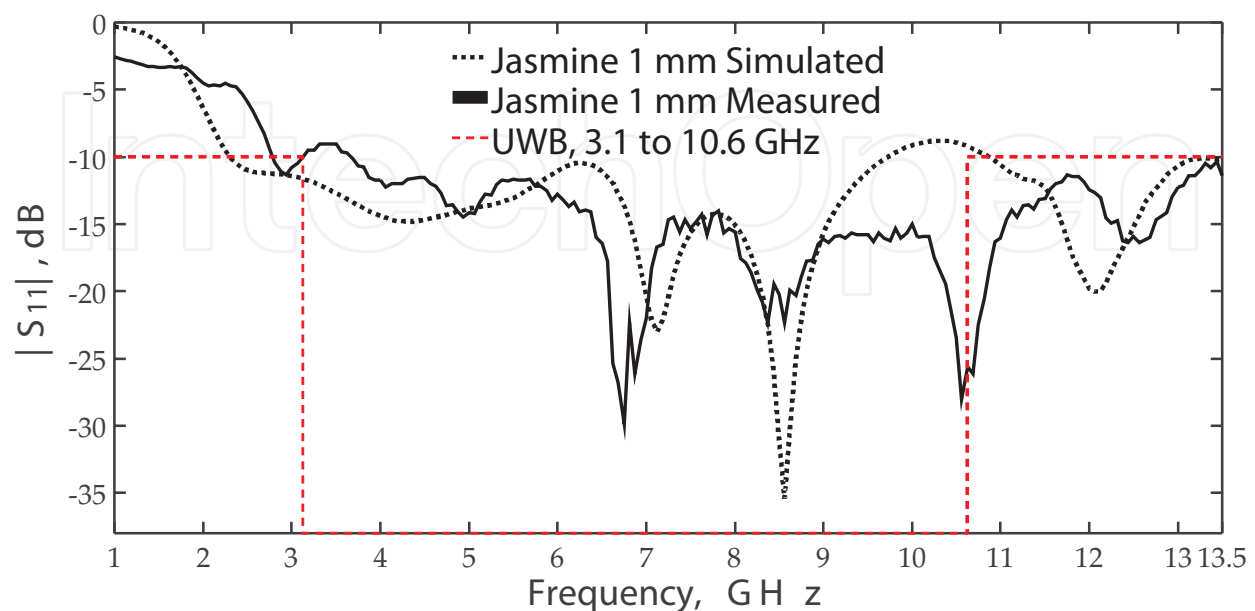


Figure 11. Comparison between simulated and measured results for jasmine flower PMA with petal length of 1 mm.

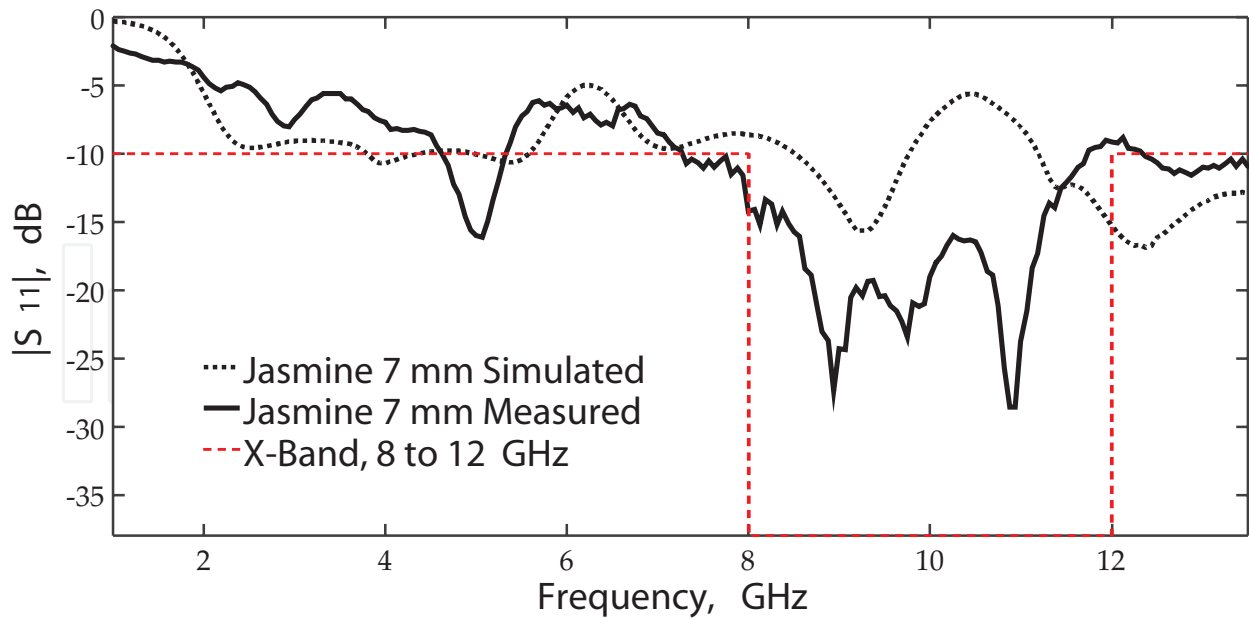


Figure 12. Comparison between simulated and measured results for jasmine flower PMA with petal length of 7 mm.

The bio-inspired antenna with a petal length of 1 mm presents a bandwidth 11% lower compared to simulations, but still cover the UWB range.

The bio-inspired geometry of a jasmine flower increases the perimeter of the antenna compared to a classical PMA and consequently the frequency behavior. The perimeter of the antenna is bigger without changing its size. In the case of petal, length of 7 mm is possible to change the resonance frequency and bandwidth to operate in the X-band range (8–12 GHz).

The **Figure 13** shows the measured values of the circular PMA and the bio-inspired antennas with petal length of 1 and 7 mm.

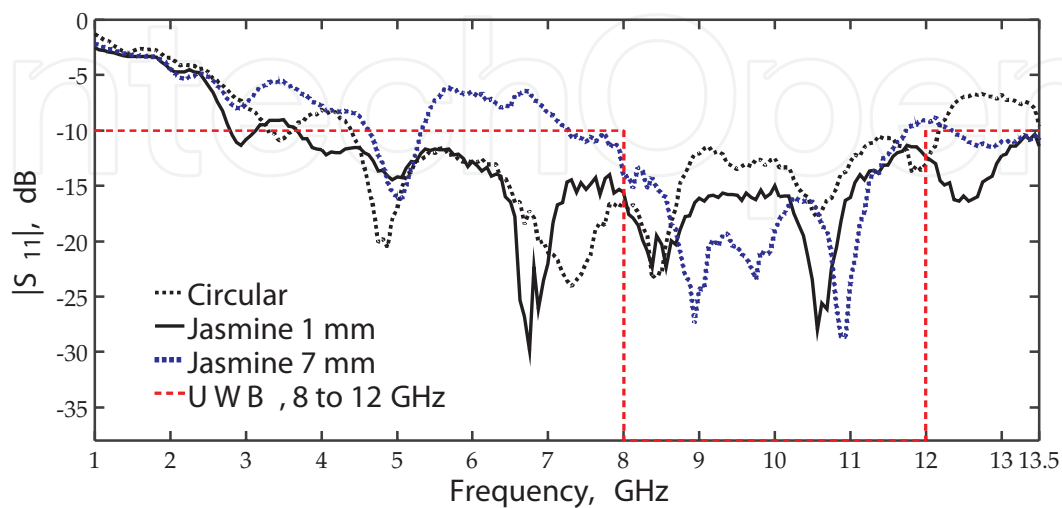


Figure 13. Comparison between measurements of $|S_{11}|$ for built printed monopole antennas: circular and jasmine flowers (1 and 7 mm).

The difference between the resonance frequencies and bandwidth of the built antennas is presented in **Table 6**.

Figure 14 shows the 3D simulated radiation patterns of the circular PMA and the bio-inspired antennas with petal length of 1 mm and 7 mm. The radiation patterns at 7.13 GHz of the circular PMA, at 7.06 GHz, of the jasmine flower with petal length of 1 mm and at 9.25 GHz of the jasmine flower with petal length of 7 mm are presented in **Figure 14(a)–(c)**, respectively. The antennas presented maximum gain in the broadside direction close to 6 dBi and omnidirectional radiation pattern.

3.3.3. Wearable ginkgo biloba leaf-shaped antenna

The ginkgo biloba is a plant of Chinese origin; its name means silver apricot and can be found on all continents. The leaves of this plant have interesting characteristics, such as good ratio between its length and width, and a geometry with a larger perimeter than Euclidean geometries. Those characteristics, in a PMA, provide a broadband antenna, with reduced dimensions, covering the lower frequency bands. This feature allows a compact antenna design and the

| | Antenna | BW (GHz) | f_1 (GHz) | f_2 (GHz) |
|---|------------------------|----------|-------------|-------------|
| 1 | Circular simulated | 7.38 | 2.31 | 9.69 |
| 2 | Circular measured | 10.69 | 2.81 | 13.50 |
| 3 | Jasmine 7 mm simulated | 11.00 | 2.50 | 13.50 |
| 4 | Jasmine 7 mm measured | 8.45 | 3.75 | 12.20 |
| 5 | Jasmine 1 mm simulated | 4.25 | 8.00 | 12.25 |
| 6 | Jasmine 1 mm measured | 3.44 | 9.25 | 11.69 |

Table 6. Comparison of frequency response and bandwidth.

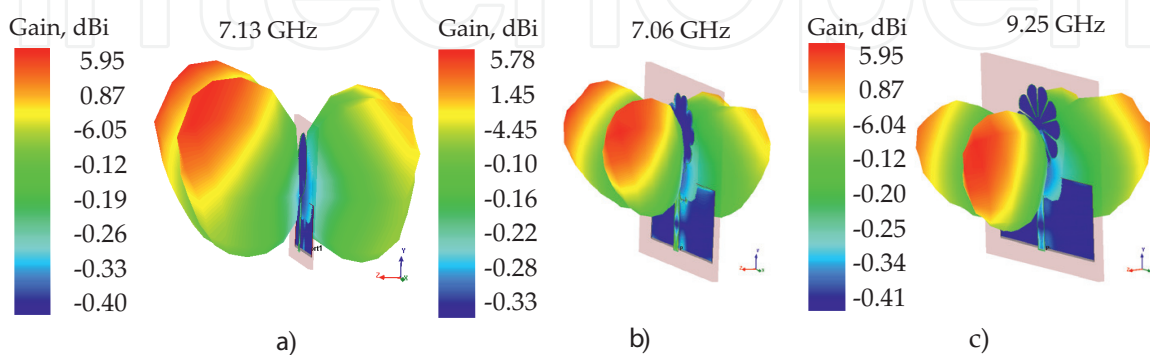


Figure 14. 3D simulated radiation patterns: (a) PMA at 7.13 GHz, (b) 1 mm jasmine flower at 7.06 GHz, (c) 7 mm jasmine flower at 9.25 GHz.

possibility of use in different frequency bands. From the determination of the perimeter, the use of geometry of ginkgo biloba leaf was applied to a broadband antenna structure, in which it was possible to run the project for an antenna that covers the frequencies of the technologies 2G, 3G and 4G.

The image of the ginkgo biloba leaf used for the proposed antenna was generated using the software MATLAB®, with values: $m = 4$, $n_1 = -0.1$, $n_2 = 0.14$, $a = 0.1$ and $b = 1$.

In **Figure 15** are shown the shape generated and the simulated structure with dimensions and, in **Figure 16**, the prototype of the proposed antenna.

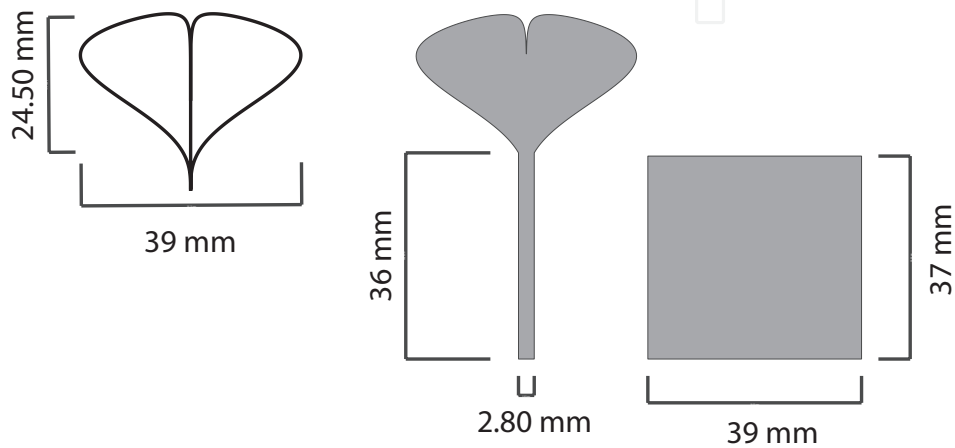


Figure 15. Simulated structure of the textile PMA ginkgo biloba.



Figure 16. Textile PMA ginkgo biloba prototype.

In **Figure 17** is shown the comparison of the values of the parameter $|S_{11}|$ measured and simulated of the PMA ginkgo biloba. As noted, the measurement and simulation show similar results, indicating convergence between the simulation and the prototype.

In **Figure 18**, the parameter $|S_{11}|$ measured of the PMA ginkgo biloba in the pocket can be seen, close of the head and hand at distance of 20 mm. As noted, the antenna used close to the body suffers interference, which promotes the shift of the frequency and bandwidth of the antenna. In **Table 7**, the measured and simulated values, resonant frequencies, and bandwidth of the bio-inspired antenna can be observed. The resonance frequencies have difference $<4.2\%$, the first frequency and bandwidth covering 2G (1850–1900 MHz), 3G (1920–1975 MHz) and 4G (LTE; 2500–2690 MHz) bands.

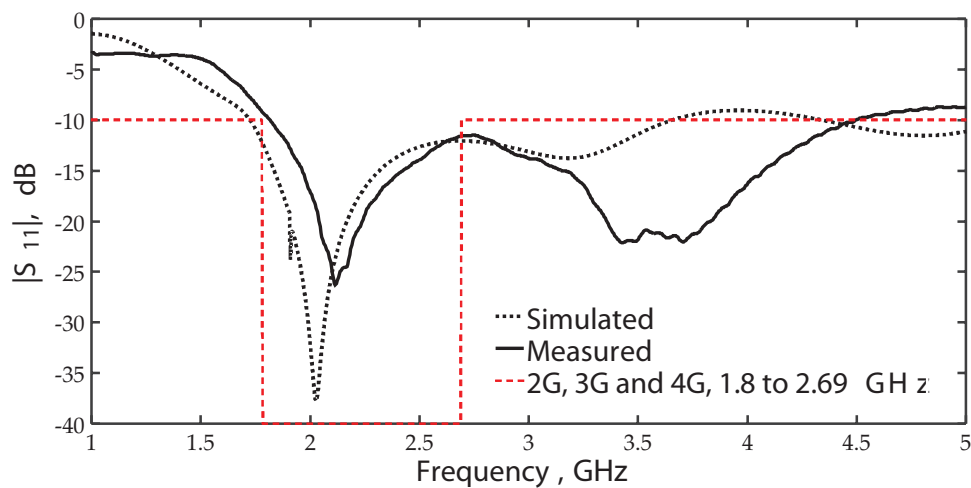


Figure 17. Simulated and measured $|S_{11}|$ parameter of the PMA ginkgo biloba.

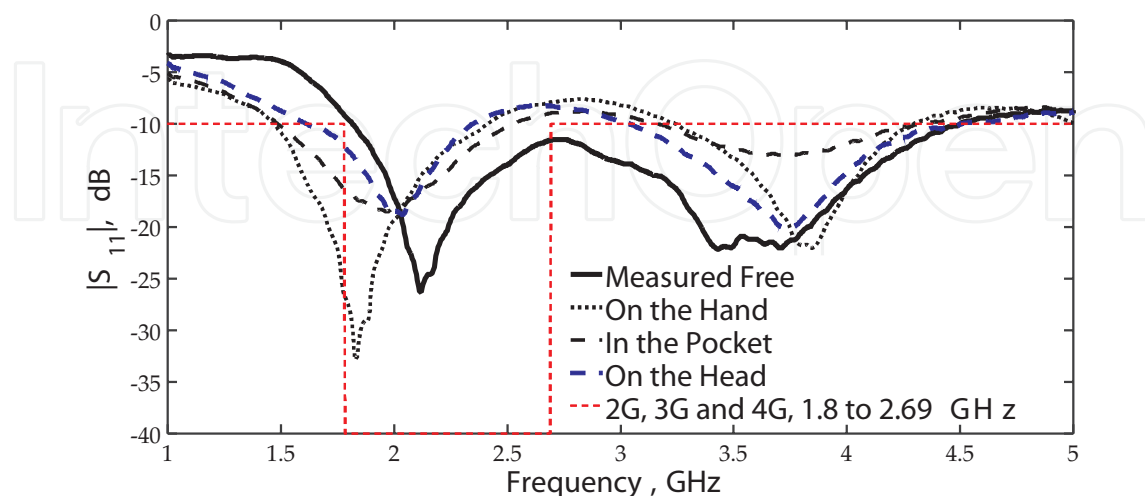


Figure 18. Simulated and measured $|S_{11}|$ parameter of the PMA ginkgo biloba with body interferences.

| | Antenna | BW (GHz) | f_1 (GHz) | f_2 (GHz) | f_0 (GHz) |
|---|--------------------|----------|-------------|-------------|-------------|
| 1 | Simulated | 3.51 | 1.73 | 5.24 | 2.03 |
| 2 | Measured | 2.70 | 1.80 | 4.50 | 2.12 |
| 3 | Measured on head | 0.73 | 1.61 | 2.34 | 2.04 |
| 4 | Measured in pocket | 1.04 | 1.49 | 2.53 | 1.97 |
| 5 | Measured on hand | 0.94 | 1.47 | 2.41 | 1.83 |

Table 7. Comparison of frequency response and bandwidth of the simulated and measured PMA ginkgo biloba.

The measurements, using the antenna nearly the head, hand, and in the pocket, showed different resonant frequencies and bandwidths. The biggest difference in the resonance frequency was observed nearly the hand, with a difference of 13.68%. The biggest difference in bandwidth was detected at the antenna close to the head, with a difference of 72.96%.

The **Figure 19** shows the 2D and 3D radiation patterns of the PMA textile ginkgo biloba at 2.12 GHz, with a maximum gain 3.16 dBi in the broadside direction. The 2D radiation pattern measured for $\Phi = 90^\circ$ was performed in semi-anechoic chamber. It can be observed that the half-power beam width (HPBW) in ($\phi = 90$) E-plane is $\sim 120^\circ$ with an omnidirectional radiation pattern. By presenting equivalent power distribution and omnidirectional radiation diagram, this antenna can be used in applications that require direct communication between devices, in which the transmitter/receiver can take various positions.

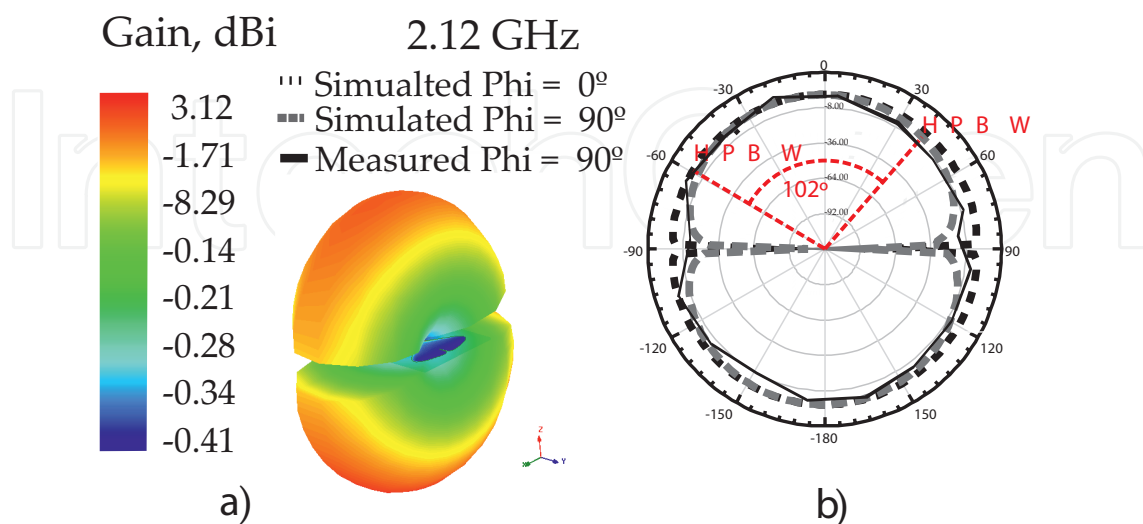


Figure 19. 2D and 3D radiation pattern of the antenna proposed.

3.3.4. Wearable *Bidens pilosa* leaf-shaped antenna

The *Bidens pilosa* is native to the Americas, but it is known widely as an introduced species of other regions. The use of geometry of *Bidens pilosa* with three leaves was applied to a broadband antenna structure, in which it was possible to run the project for an antenna that covers the WLAN range at 2.40 GHz (2.40–2.4835 GHz).

Based on the perimeter of a classical circular antenna, it is possible to design the bio-inspired textile patch antenna with three elliptical leaves using the Gielis formula. Thus, the leaves are generated by the parameters $n_1 = 2$, $m = 400$, n_2 and $n_3 = 1200$, a and $b = 1$. The final structure obtained total perimeter of 143.3 mm.

In **Figure 20** are shown the circular patch simulated, the dimensions of the single leaf used, the simulated dimensions of the bio-inspired array antenna and the prototype, respectively. In the simulation and the prototype, the under leaf was inclined at 20° , and the down leaves were inclined at 40° in relation to the geometry of *Bidens pilosa*, in order to provide fine-tuning of the resonance frequency.

Figure 21 shows a comparison between the simulated $|S_{11}|$ parameter for the circular patch antenna and the bio-inspired textile antenna. The circular patch antenna obtains a bandwidth of 140 MHz and the bio-inspired wearable patch antenna of 130 MHz. Both antennas have bandwidth that fully covers the required frequency range for WLAN technology. However, the bio-inspired array patch antenna presents a reduction of total length in 33.61% and width in 52.01% compared to the circular patch antenna.

Figure 22 shows a comparison between the simulated and measured $|S_{11}|$ parameter for the bio-inspired wearable textile patch antenna proposed. As it can be observed, the simulated and measured prototypes show a convergent behavior. The measured bandwidth is 8.33% narrower than the simulated values, but still fully covering the WLAN band.

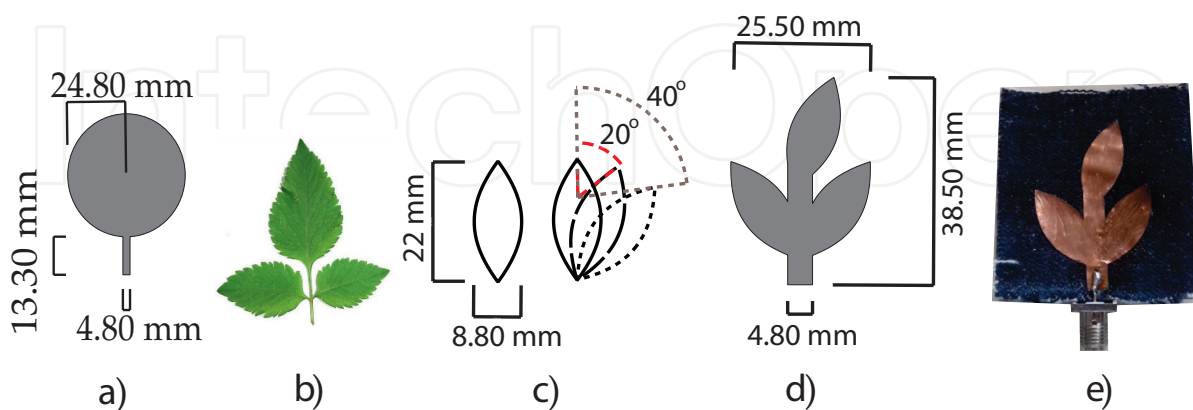


Figure 20. (a) Circular patch simulated (b) leaves array of *Bidens pilosa*, (c) single elliptical leaf, (d) bio-inspired patch antenna simulated, (e) bio-inspired prototype.

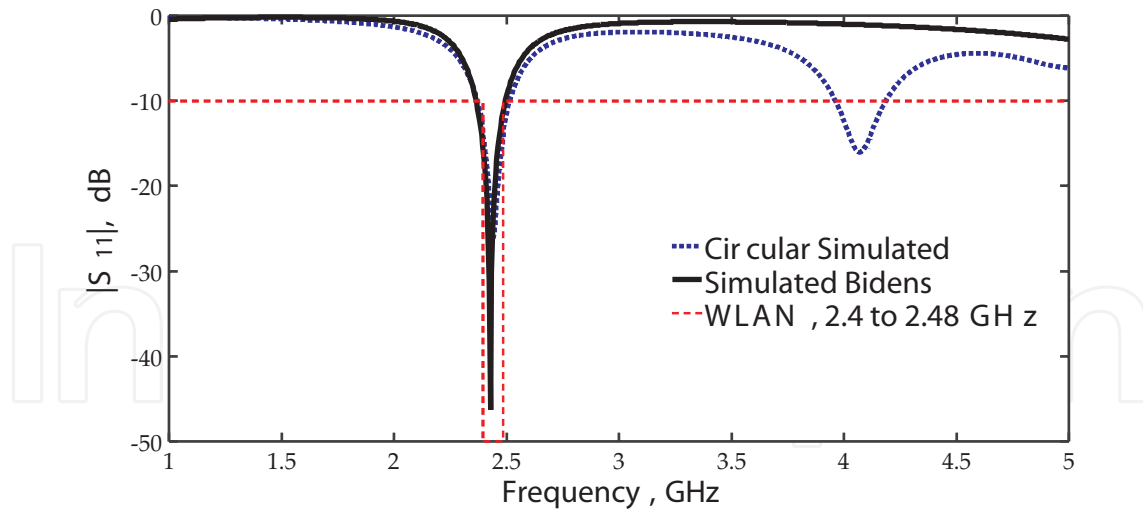


Figure 21. Comparison between $|S_{11}|$ parameter of the circular patch and the bio-inspired textile antenna.

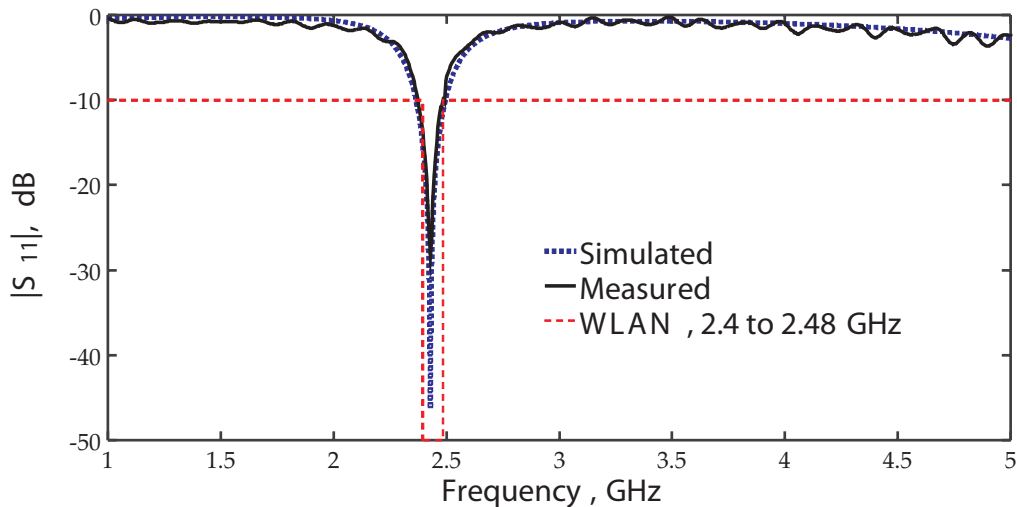


Figure 22. Comparison of $|S_{11}|$ parameter simulated and measured of *Bidens pilosa* patch antenna.

In Figure 23 is illustrated the radiation pattern in 3D and 2D with the half power beam width and relative front-to-back (F/B) for the simulated bio-inspired textile array antenna. The 2D radiation pattern measured for $\Phi = 90^\circ$ was performed in semi-anechoic chamber. It can be noted that the antenna presents an end-fire direction with maximum gain of 6.71 dBi, HPBW = 90° (indicated by the letters 'A' and 'B') and F/B = 21 dB.

In Figure 24 is shown the simulated current density of the bio-inspired textile antenna and the circular antenna at 2.43 GHz. It can be observed that the surface current is more distributed on the edges than on the center of the patch. The current density of the circular patch is 5.86 A/m^2 , and the bio-inspired is 40.06 A/m^2 . Therefore, the bio-inspired antenna presents a higher concentration of the surface current in a smaller physical area of the antenna.

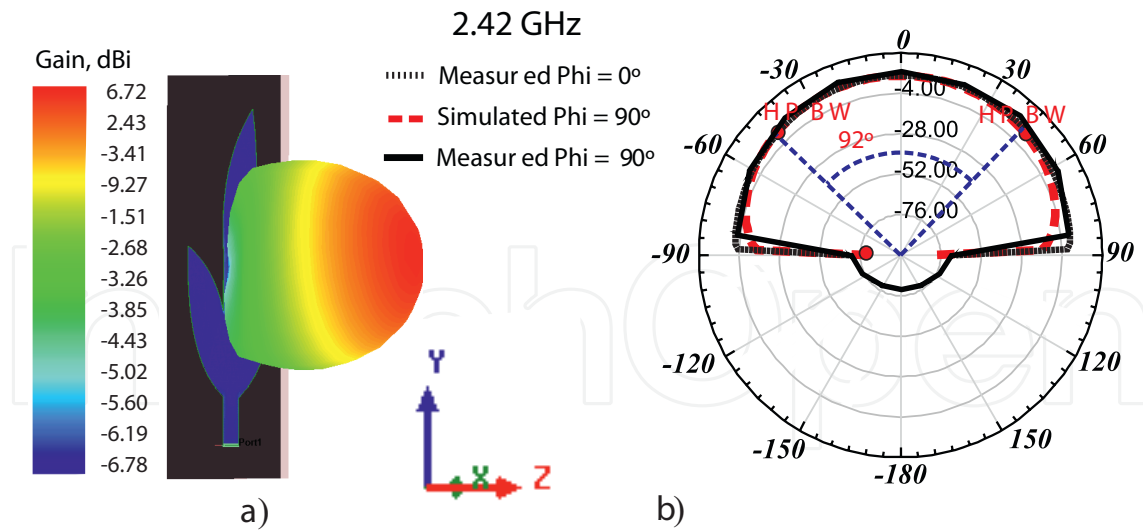


Figure 23. Radiation pattern of the bio-inspired textile antenna: (a) 3D with antenna structure, (b) 2D with HPBW and relative F/B.

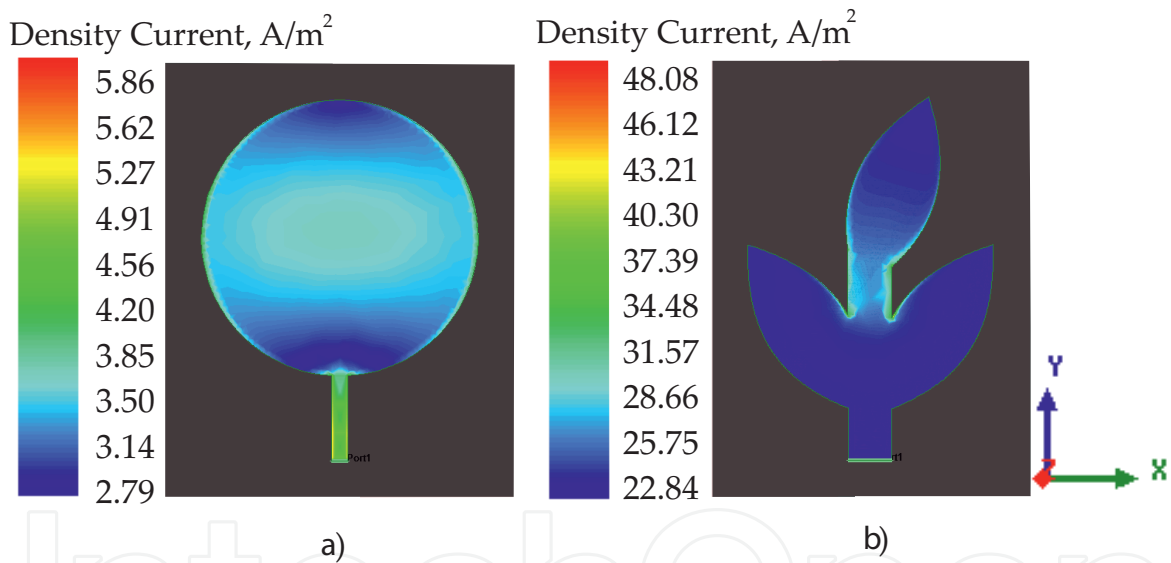


Figure 24. Current density distribution: (a) circular patch antenna, (b) bio-inspired textile patch antenna.

4. Conclusion

In this chapter, we have described some trends for design innovative bio-inspired microstrip antennas. The methods of analysis, manufacturing, and measurement have presented considering different dielectric materials (rigid and flexible) for the manufacture of the antennas. The unique properties of space filling and self similarity naturally result in more compact and multiband behavior antennas. Consequently, these antennas have their gain reduced, which in many wireless applications are undesirable characteristics. On the other hand, as observed on the last case, the bio-inspired antenna presents a higher concentration of the surface current in

a smaller physical area compared to classical geometries with esthetic appeal. The bio-inspired microstrip antennas have few design variables and smooth responses in the region of interest of these design variables, which facilitates all steps of the design methodology. These characteristics open a vast research field for wearable embedded antennas.

Author details

Alexandre Jean René Serres^{1*}, Georgina Karla de Freitas Serres¹, Paulo Fernandes da Silva Júnior¹, Raimundo Carlos Silvério Freire¹, Josiel do Nascimento Cruz¹, Tulio Chaves de Albuquerque¹, Maciel Alves Oliveira¹ and Paulo Henrique da Fonseca Silva²

*Address all correspondence to: alexandreserres@gmail.com

1 Electrical Engineering – COPELE, Federal University of Campina Grande – UFCG, Campina Grande, Brazil

2 Electrical Engineering, Federal Institute of Paraiba – IFPB, Paraiba, Brazil

References

- [1] R.A. Sainati, *Cad of microstrip antennas for wireless applications*, Artech House, Norwood, MA, USA, 1996.
- [2] Z. N. Chen, *Antennas for Portable Devices*. Chichester: John Wiley & Sons, 2007. 290 p.
- [3] Z. N. Chen and M.Y.W. Chia, *Broadband planar antennas: design and applications*. John Wiley & Sons, Ltd, Chichester, England, 2006.
- [4] K.-L. Wong, *Compact and broadband microstrip antennas*, John Wiley & Sons, Inc., New York, USA, 2002.
- [5] 5G Americas, *5G Americas White Paper on 5G Spectrum Recommendations- April 2017*, [Online]. Available: http://www.5gamericas.org/files/9114/9324/1786/5GA_5G_Spectrum_Recommendations_2017_FINAL.pdf. [Accessed: 12- Jun- 2017].
- [6] C. A. Balanis. *Antenna Theory*. 3rd ed. Arizona: Wiley; 2009. 941 p.
- [7] R. Garg, P. Bhartia, I. Bahl, and A. Ittipiboon, *Microstrip antenna design handbook*, Artech House, Boston, USA, 2001.
- [8] W. L. Stutzman, *Antenna Theory and Design*, 2 ed. New York: John Wiley & Sons, 1998. 598 p.
- [9] G. Kumar and K. P. Ray, *Broadband microstrip antennas*, Artech House, Boston, Mass, USA, 2003.
- [10] Yoseph Bar-Cohen. *Biomimetics: Biologically Inspired Technologies*. Boca Raton, FL: Taylor and Francis; 2006

- [11] Falko Dressler and Ozgur B. Akan. A survey on bio-inspired networking. *Computer Networks*. 2010;**54**(6):881-900. DOI: 10.1016/j.comnet.2009.10.024
- [12] J.A. Flint. A biomimetic antenna in the shape of a bat's ear. *IEEE Antennas and Wireless Propagation Letters*. 2006;**5**(1):145-147. DOI: 10.1109/LAWP.2006.873940
- [13] Nader Behdad, Mudar A. Al-Joumayly and Meng Li. Biologically Inspired Electrically Small Antenna Arrays With Enhanced Directional Sensitivity. *IEEE Antennas and Wireless Propagation Letters* . 2011;**10**:361-364. DOI: 10.1109/LAWP.2011.2146223
- [14] Khabat Ebnabbasi. A Bio-Inspired Printed-Antenna Transmission-Range Detection System. *IEEE Antennas and Propagation Magazine*. 2013;**55**(3):193-200. DOI: 10.1109/MAP.2013.6586661
- [15] G.H. Huff. Biologically-inspired vascular antenna reconfiguration mechanism. *Electronics Letters*. 2011;**47**(11):637 - 638. DOI: 10.1049/el.2011.0383
- [16] Xiao-Feng Bai, Shun-Shi Zhong and Xian-Ling Liang. Leaf-shaped monopole antenna with extremely wide bandwidth. *Microwave and Optical Technology Letters*. 2006; **48**(7):1247-1250. DOI: 10.1002/mop.21668
- [17] Soh Fujita, Manabu Yamamoto and Toshio Nojima. A study of a leaf-shaped bowtie slot antenna for UWB applications. In: IEEE, editor. *International Symposium on Antennas and Propagation (ISAP)*; 29 Oct.-2 Nov. 2012;Nagoys: p. 830-833.
- [18] A. N. Askarpour, A. Gholipour and R. Faraji-Dana. A Band-Notched Tulip Antenna for UWB Applications. In: *38th European Microwave Conference*; 27-31 Oct. 2008; Amsterdam: IEEE; 2008. p. 881-884. DOI: 10.1109/EUMC.2008.4751594
- [19] F. M. Tanyer-Tigrek, D. P. Tran, I. E. Lager and L. P. Ligthart. Wide-band tulip-loop antenna. In: *3rd European Conference on Antennas and Propagation*; 23-27 March 2009; Berlin: IEEE; 2009. p. 1446-1449.
- [20] S. R. Patre and S. P. Singh. MIMO antenna using castor leaf-shaped quasi-self-complementary elements for broadband applications. In: *IEEE MTT-S International Microwave and RF Conference (IMaRC)*; 10-12 Dec. 2015; Hyderabad: IEEE; 2015. p. 140-142. DOI: 10.1109/IMaRC.2015.7411400
- [21] P. F. Silva Júnior, P. H. da F. Silva, A. J. R. Serres, J. C. Silva and R. C. S. Freire. Bio-inspired design of directional leaf-shaped printed monopole antennas for 4G 700 MHz band. *Microwave and Optical Technology Letters*. 2016;**58**(7):1529-1533. DOI: 10.1002/mop.29853
- [22] D. M. Sullivan, *Electromagnetic Simulation Using the FDTD Method*. New York: Wiley: IEEE Press, 2000.
- [23] MANDELBROT, B. B. *The fractal geometry of nature*. 3. ed. Nova York: W. H. Freeman and Co., 1982. 468p.
- [24] FALCONER, K. *Fractal geometry: mathematical foundations and application*. 2. ed. Londres: Wiley, 2003. 337p.

- [25] Mishra, J. and Mishra, S. L-Systems Fractals. Amsterdam, Netherlands: Elsevier, 2007. 274p.
- [26] Barnsley, M. Fractals Everywhere. San Diego: Academic Press, 1988. 394 p.
- [27] Johan Gielis. A generic geometric transformation that unifies a wide range of natural and abstract shapes. American Journal of Botany. 2003;**90**(3):333-338. DOI: 10.3732/ajb.90.3.333
- [28] E. E. C. Oliveira, P. H. da F. Silva, A. L. P. S. Campos, S. G. Silva. Overall size antenna reduction using fractal elements. Microwave and Opt Technol Letters. 2009;**51**(3):671-675. DOI: 10.1002/mop

IntechOpen

